TMS-induced neuronal plasticity enables targeted remodeling of visual cortical maps

Vladislav Kozyrev[a,1,2], Robert Staadt[a,1], Ulf T. Eysel[b], and Dirk Jancke[a,3]

[a]Optical Imaging Group, Institut für Neuroinformatik, Ruhr University Bochum, 44780 Bochum, Germany; and [b]Department of Neurophysiology, Ruhr University Bochum, 44780 Bochum, Germany

Transcranial magnetic stimulation (TMS) has become a popular clinical method to modify cortical processing. The events underlying TMS-induced functional changes remain, however, largely unknown because current noninvasive recording methods lack spatiotemporal resolution or are incompatible with the strong TMS-associated electrical field. In particular, an answer to the question of how the relatively unspecific nature of TMS stimulation leads to specific neuronal reorganization, as well as a detailed picture of TMS-triggered reorganization of functional brain modules, is missing. Here we used real-time optical imaging in an animal experimental setting to track, at submillimeter range, TMS-induced functional changes in visual feature maps over several square millimeters of the brain's surface. We show that high-frequency TMS creates a transient cortical state with increased excitability and increased response variability, which opens a time window for enhanced plasticity. Visual stimulation (i.e., 30 min of passive exposure) with a single orientation applied during this TMS-induced permissive period led to enlarged imprinting of the chosen orientation on the visual map across visual cortex. This reorganization was stable for hours and was characterized by a systematic shift in orientation preference toward the trained orientation. Thus, TMS can noninvasively trigger a targeted large-scale remodeling of fundamentally mature functional architecture in early sensory cortex.

sensory cortex plasticity | remodeling orientation maps | voltage-sensitive dye imaging | transcranial magnetic stimulation | state-dependent response variability

Despite the fact that the functional layout of early sensory cortical areas appears largely fixed in the adult central nervous system, there is also evidence that cortical networks can specifically be remodeled through experience or perceptual training (1–3). However, the underlying mechanisms and the conditions under which remodeling can be enhanced are still under debate. Transcranial magnetic stimulation (TMS) holds promise as a tool for noninvasively facilitating cortical reorganization (4–7). At the behavioral level, repetitive TMS enables long-lasting functional alterations in the visual system when used in combination with perceptual learning protocols (8, 9). For example, high-frequency (10 Hz) TMS over human primary visual cortex (V1) can improve contrast sensitivity of amblyopic ("lazy-eye") patients (8) and modulate performance in visual detection tasks (10). However, the neuronal basis of TMS-induced changes and the presumed modifications in functional connectivity are unknown because online monitoring methods using neuroimaging techniques applicable in humans (e.g., fMRI, MEG, EEG) are limited in either spatial or temporal resolution, or both (11–13).

Here we used voltage-sensitive dye (VSD) imaging in anesthetized cats and applied TMS over V1 followed by prolonged (30-min) visual stimulation. Our goal here was to create a simple model of passive, nonattentional, visual training (14). The VSD transforms changes in neuronal membrane voltage into fluorescent signals, providing micrometer and microsecond resolution for imaging neocortical functional activity (15), and is immune to TMS-induced electromagnetic artifacts (16).

Results

Experiments started with acquisition of orientation maps followed by 30 min of TMS. In most experiments, maps were again evaluated directly after TMS before visual stimulation started with prolonged exposure to a single orientation. Fig. 1A shows two examples of V1 orientation maps before (pre-) and after (post-) treatment with high-frequency 10-Hz TMS and subsequent visual stimulation. Before TMS, the recorded maps displayed the typical layout (Fig. 1A, Left), characterized by regular representation of different orientation angles around "pinwheel" centers (17). Next, we inspected the maps following 10-Hz TMS and prolonged visual exposure to a single orientation, excluding times directly after visual stimulation to avoid overlap with early adaptation effects (18). We detected that maps were dominated by the representation of the stimulated orientation, i.e., horizontal in the example in Fig. 1A, Top. Starting from a map with roughly equal representation of all orientations, the cortical area representing horizontal (orange/reddish/colors) increased by 28.9%, here measured 1–2.5 h post visual stimulation. To verify that the plastic cortical change was specific to visual stimulation, we used different orientations in different experiments. In the second example shown (Fig. 1A, Bottom), stimulus orientation was 90°, and orientation was dominance-shifted

Significance

Transcranial magnetic stimulation (TMS) holds promise as a tool for noninvasively facilitating plastic changes in cortical networks. However, highly resolved visualization of its modulatory effects remains elusive because current neuroimaging techniques applicable in humans are limited in spatiotemporal resolution. Here we used an imaging approach with voltage-sensitive dye and tracked, at submillimeter range, TMS-induced plastic changes across cat primary visual cortex. We show that high-frequency 10-Hz TMS induces a state where visual cortical maps are transiently "destabilized." In turn, the cortex was sensitized to a bias in input—here imposed by prolonged exposure to a single visual orientation—and primed to relearn connectivity patterns. These findings implicate an early post-TMS time window for promising therapeutic interventions through TMS.

[1]V.K. and R.S. contributed equally to this work.

[2]Present address: Decision and Awareness Group, Cognitive Neuroscience Laboratory, German Primate Center–Leibniz Institute for Primate Research, 37077 Göttingen, Germany.

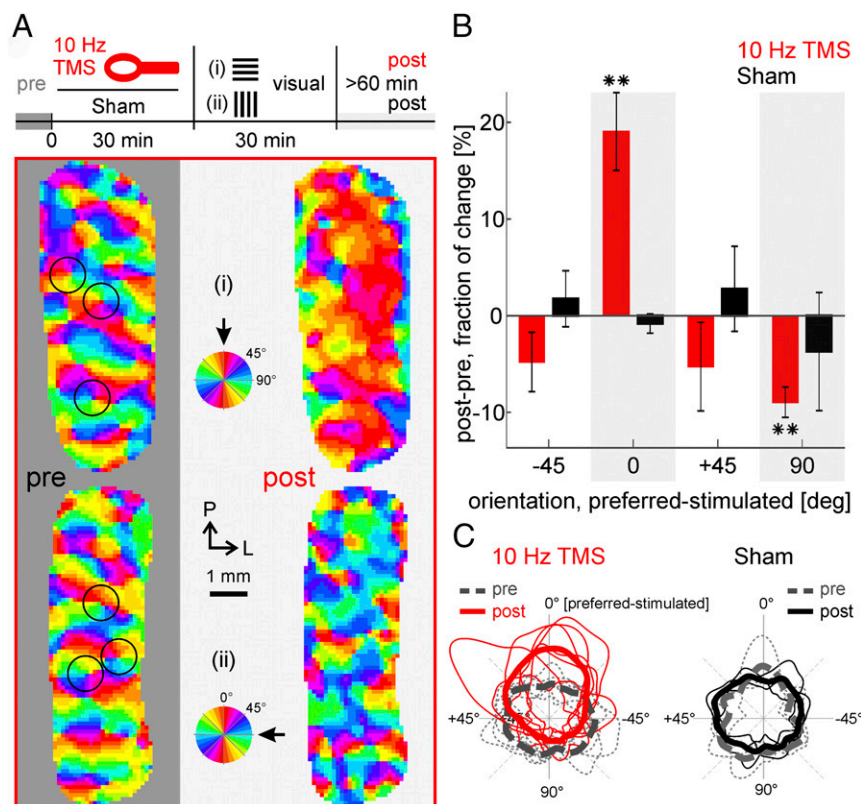[3]To whom correspondence should be addressed. Email: dirk.jancke@rub.de.

Fig. 1. Targeted remodeling of cortical orientation maps after 10-Hz TMS and visual stimulation. (*A, Top*) Stimulation procedure, 30 min of 10-Hz TMS (or sham TMS) followed by 30 min of visual stimulation with a single orientation; two different orientations (i/ii) are shown. (*Bottom*) Orientation maps of two experiments (average over 8–17 trials). Colors denote each pixel's orientation preference before (*Left*) and after (>60 min) visual stimulation (*Right*); arrows point to stimulated orientation. Examples of pinwheel locations encircled in black. L, lateral; P, posterior. (*B*) Percentage of change in representation (mean across experiments) after 10-Hz TMS (red, $n = 7$) and after sham (black, $n = 3$); error bars indicate SEM. Values were binned to cardinal and oblique orientations and centered (on zero) relative to the orientation used for visual stimulation. **$P < 0.01$, one-sample t test. An eight-way ANOVA test showed that there is a significant difference between 10-Hz TMS and sham conditions in at least one pair of changes ($P < 0.0001$). Post hoc multiple comparison analysis revealed that this difference was significant at the stimulated (0°) orientation ($P = 0.0453$). (*C*) Polar plots of the distribution of orientation preference for the individual experiments (thin lines) and their mean (thick lines), with zero relative to the trained orientation.

toward vertical orientations (bluish/greenish colors), again revealing an increased (18.6%) representation of the stimulated and neighboring orientations. Across all experiments, the relative augmentation of regions representing the stimulated orientation was $19.0 \pm 4.0\%$ SEM (Fig. 1*B*; $P = 0.0257$, one-sample t test, Bonferroni-corrected for eight comparisons, $n = 7$ experiments), with simultaneous reduction of pixels with orientation preference orthogonal (i.e., 90°) to the stimulated orientation (Fig. 1*B*, $P = 0.0099$, one-sample t test, Bonferroni-corrected for eight comparisons, $n = 7$). No significant changes were observed in cases where visual stimulation followed sham TMS (Fig. 1*B*, black bars, $n = 3$). Fig. 1*C* summarizes these findings in a polar graph (*SI Appendix, SI Methods*) for the individual experiments (thin lines). On average the cortical reorganization was evident in the biased occurrence of orientations neighboring the visually trained orientation after 10-Hz TMS (Fig. 1*C*, red lines in *Left* graph, average outlined in bold), notably different from pretreatment conditions (outlined stippled gray), as well as from sham pre and post visual stimulation conditions (Fig. 1*C*, *Right* graph). Further analysis revealed that the increased representation of the stimulated orientation was not randomly recruited—apparent by a systematic shift in orientation preference of the neighboring orientation domains toward the stimulated orientation (Fig. 2).

The above findings indicate that the key mechanisms responsible for the observed remodeling lie in the immediate high-frequency TMS effects. Next, we therefore directed our analysis to the time window straight after TMS treatment ("post 10-Hz TMS"). Fig. 3*A*, *Left* depicts orientation map layout, assigning reproducibility values (i.e., trial-to-trial circular variance; see *SI Appendix, SI Methods*) to all pixels. If a given pixel consistently responded strongest to the same orientation in each trial, it has a high reproducibility value (brightness in maps indicates degree of reproducibility) with low values (dark) for inconsistent preferred orientation across trials. Note that this method faithfully captures the location of pinwheel centers (see dark local spots within the three encircled examples) because pinwheel pixels cover (i.e., average) neurons tuned to different orientations at closest distance

(17). Strikingly, following 10-Hz TMS, the reproducibility of the pixels' orientation preferences was strongly reduced compared with the pre-TMS map (Fig. 3*A*, *Right*).

Furthermore, the rising phase of the VSD includes a small downturn ("notch"; Fig. 3*B*, gray trace), which was proposed to reflect inhibitory processes that sharpen orientation tuning (19). We found the notch diminished after 10-Hz TMS and a subsequently increased amplitude of cortical activity (Fig. 3*B*; compare gray and bluish traces in encircled region and thereafter). Consistent with the present results, we previously demonstrated that 10-Hz TMS produces an excitatory cortical state where suppression is weakened, leading to the disappearance of the notch and subsequent increase in evoked activity levels with decreased orientation-specific response components (16).

In addition, pixels with low reproducibility revealed a substantial loss in modulation depth (Fig. 3*C*, $P = 0.0138$, paired t test, $n = 5$ experiments, in which we imaged directly after 10-Hz TMS). In other words, the difference between preferred and orthogonal responses [and thus selectivity (20)] was reduced compared with pixels with high reproducibility. To further confirm that the effects we observed were specific to the TMS intervention, we tracked mean reproducibility values of pre- and post-TMS conditions after 10-Hz TMS and sham controls for each individual experiment (Fig. 3*D*). Reproducibility did not significantly change after sham TMS (Fig. 3*D*; $P = 0.4995$, paired t test, $n = 4$ experiments). In contrast, reproducibility was significantly reduced after 10-Hz TMS (Fig. 3*D*; $P = 0.0155$, paired t test) in all experiments, and this reduction was significantly different from sham conditions ($P = 0.0086$, nonpaired t test). These results validate 10-Hz TMS induction of increased variability and also suggest increased decorrelation of responses across the entire neuronal populations. To quantify the effect on the correlational structure of orientation maps, we correlated averages of resampled single-trial maps (bootstrap, 1,000 iterations) with the mean map for each orientation (Fig. 3*E*). The matrices displayed the expected diagonal of highest-correlation coefficients across maps of the same orientation. After 10-Hz TMS these
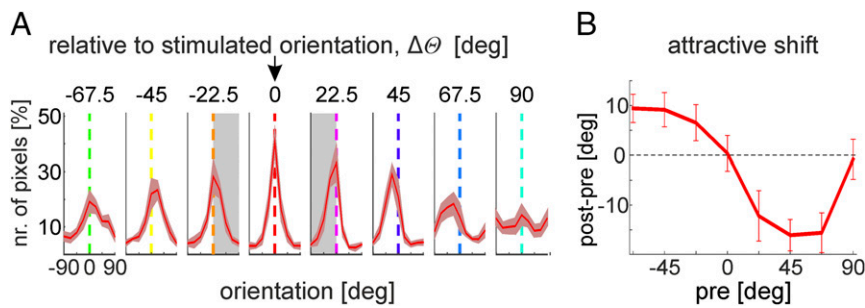
NEUROSCIENCE

Fig. 2. Attractive shift toward stimulated orientation. (*A*) Change in orientation preference (i.e., difference between pre vs. post, i.e., 10-Hz TMS and visual stimulation, >60 min) calculated for different orientation domains (see colored lines, orientation bins on top) relative to the stimulated orientation (ΔΘ = zero) for each pixel. Curves show mean across experiments (*n* = 7), shaded colored regions indicate SEM. Gray background areas sketch attraction toward stimulated orientation. (*B*) Summary of *A*; each data point represents mean orientation shift within each curve in *A*. Error bars indicate SEM.

correlations strongly declined (Fig. 3*E*, *Top*; $P = 0.0078$ paired Wilcoxon signed-rank test, $n = 5$ experiments). This decline was again significant in contrast to sham conditions ($P = 0.0281$, Wilcoxon rank-sum test), where orientation maps maintained initial response correlations (Fig. 3*E*, *Bottom*; $P = 0.1484$, paired Wilcoxon signed-rank test, $n = 4$ experiments). We conclude that the observed decline in reproducibility indicates a high-frequency TMS-induced state, in which the cortex is less suppressed, thus more excitable, and exhibits decreased orientation selectivity and decorrelation of neuronal responses: these phenomena together seem to set the ground for remodeling of the maps.

Do neurons after remodeling, particularly those with newly acquired orientation preference, display consistent orientation tuning? Fig. 4 (red solid line) depicts the tuning curve for pixels that coded for the stimulated orientation before the 10-Hz TMS intervention, as a Gaussian fit through values across all experiments. The half width at half height (45.1°) was comparable to tuning width obtained before TMS treatment (42.9°, gray curve, calculated across pixels with preference to stimulated orientations) and in the range as reported in a previous VSD-imaging study when averaging over hundreds of milliseconds (19).

Importantly, the tuning width of pixels including neurons that underwent remodeling (stippled red curve) was similar (43.7°) to that of pixels that maintained their preference throughout the experiment, altogether suggesting consistent tuning for the newly acquired orientation after reorganization of the maps.

To finally test the hypothesis that map remodeling was specifically facilitated by 10-Hz TMS-induced increase in excitability, we performed TMS using a 1-Hz protocol, proposed to act dominantly suppressive (13, 16, 21, 22). Neither remodeling nor significant shifts in orientation preference ($P = 0.2973$, repeated measures ANOVA, across all orientations, Greenhouse–Geisser-corrected) were found when visual stimulation was applied after TMS with 1 Hz (Fig. 5 *A–D*). Computing amplitude differences of visually evoked activity between pre- and immediate post-TMS conditions we found that activity after 1-Hz TMS was significantly reduced in comparison with 10-Hz TMS (Fig. 5*E*). Moreover, post 10-Hz correlations across maps and map reproducibility were significantly lower compared with post 1-Hz TMS (Fig. 5 *F* and *G*, all orientations combined), further suggesting that the observed remodeling was specifically facilitated by high-frequency
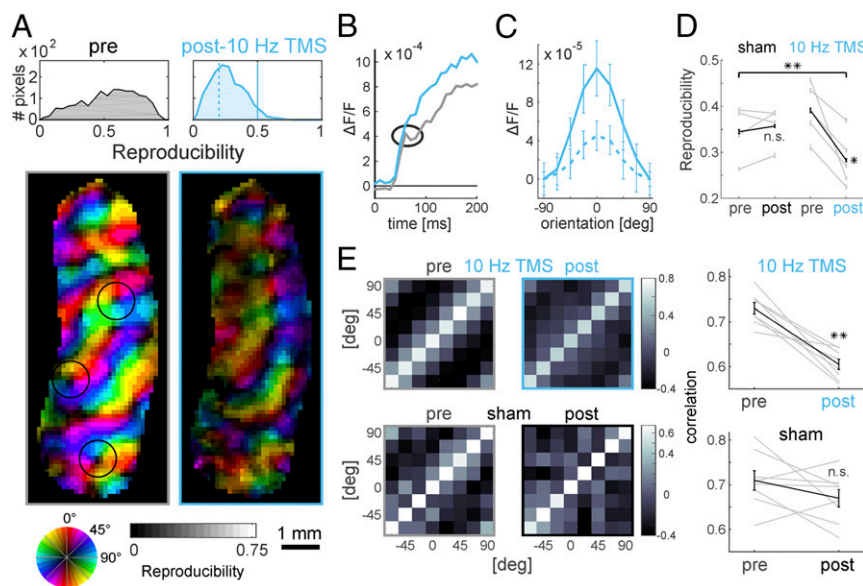
Fig. 3. Increased response variability, decrease in orientation selectivity, and reduced correlation across orientation maps after 10-Hz TMS. (*A*) Orientation map weighted with reproducibility, before 10-Hz TMS (pre) and directly after (post 10-Hz TMS). Hue represents reproducibility values; see color bar. Histograms show distribution of all pixels. (*B*) Time course of responses. Spatial average across pixels of the maps shown in *A*, including responses to all orientations. Black circle marks notch present before TMS (gray) and diminished thereafter (blue). (*C*) Orientation tuning of pixels with low reproducibility (0–0.2, as indicated in *A*, *Right*, on *Top*, stippled line) and high reproducibility (0.5–0.7, solid line). Each pixel's response amplitude to different orientations was calculated, centered on its preferred orientation; mean across five experiments (normalized). (*D*) Mean reproducibility across maps before interventions (pre) and directly after (post) 10-Hz TMS or sham, respectively; individual experiments, gray lines, averages in black. **$P < 0.01$, *$P < 0.05$, *t* test. (*E*) Matrices of correlation coefficients between pairs of orientation maps; for each experiment and each orientation the median correlation coefficient of 1,000 iterations was calculated (see text). Matrices depict mean across five and four experiments (*Top* and *Bottom*, respectively). (*Right*) Values across the diagonals of the matrices (gray lines) and their average. Error bars indicate SEM. **$P < 0.01$, Wilcoxon signed-rank test.

Fig. 4. Remodeled orientation tuning after 10-Hz TMS and visual stimulation. Orientation tuning (same conventions as in Fig. 3*C*) for pixels that preserved preference to the stimulated orientation (solid red line), for pixels that newly acquired (i.e., remodeled) preference for the stimulated orientation (stippled red line), and for pixels before interventions (gray line). Each line is a Gaussian fit through data points of the corresponding conditions. Average across stimulated orientations; mean across seven experiments. Error bars indicate SEM.

10-Hz TMS along with induced decorrelation and increase of response variability.

Discussion

In previous studies, intracortical microstimulation (23, 24) or retinal lesions were used (3, 25–28) to show that the intrinsic horizontal cortical network has the potential to undergo remapping of orientation preference. The latter approach revealed slowly developing and long-lasting effects after weeks and months of recovery within the deprived cortical region (3, 25, 26, 28). How stable are the reorganized maps in our case, where we noninvasively applied only a brief period of cortical perturbation by TMS? We found map stability was preserved for up to 6 h after TMS and visual stimulation (median across all experiments was 2.5 h), i.e., for as long as we could record reliable optical signals (see *Methods*). Using 2-photon imaging it has been shown that spine growth and retraction, as well as de novo formation of axonal boutons, can occur over tens of minutes (29), contributing to massive restructuring of neuronal circuits (30), which makes it likely that the here observed remodeling might be associated with structural plasticity. We speculate that a long-lasting establishment of functional reorganization may, however, also require repeated sessions of high-frequency TMS (12, 31) to counteract the tendency of neurons that underwent plastic changes to regain their pretreatment response properties (32). Additionally, the fact that we measured effects under anesthesia must be taken into account, as cortical responsiveness can be changed greatly, dependent on behavioral conditions (33).

Whether TMS-induced remodeling of orientation maps promotes existing intrinsic cross-connectivity through unmasking of latent inhibitory connections (26, 34, 35) or, rather, incorporates plastic changes across thalamic afferents (36) remains to be clarified. On the one hand, high-frequency TMS pulses facilitate cortical disinhibition (37, 38) and, consequently, excitability. Moreover, repetitive 10-Hz magnetic stimulation in entorhinohippocampal slice cultures was shown to reduce GABAergic synapt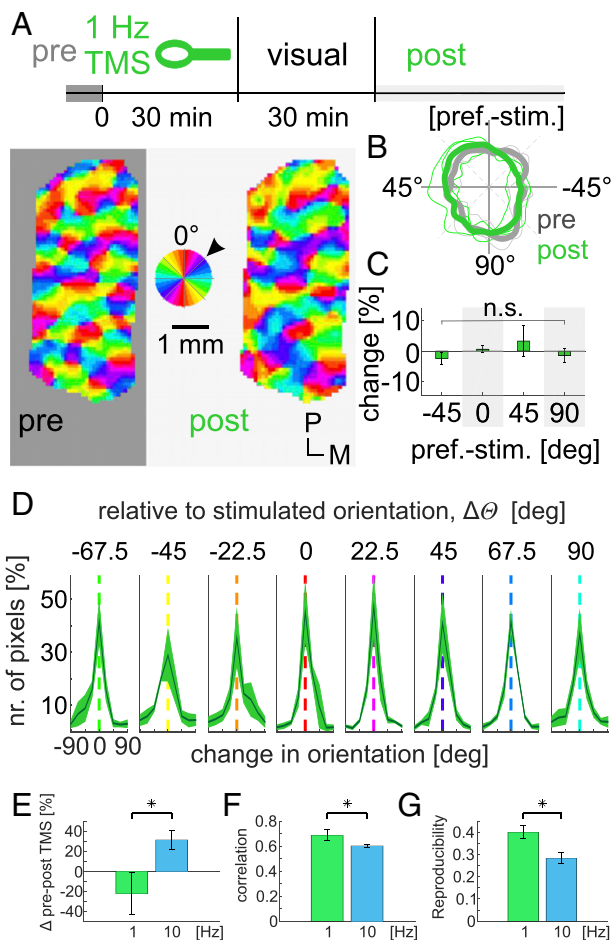ic strength (22). Hence, the here found 10-Hz TMS-triggered attractive shift in orientation preference toward the stimulated orientation could result from weakening of lateral suppression (39). On the other hand, increased excitability was recently proposed to evolve from TMS-induced cortico–subcortical loops (40) based on the observation of a rebound excitation phase following TMS (16, 40). Thus,

postulating that increased excitability predisposes toward remodeling, the dominance of the visually stimulated orientation could also incorporate TMS-enhanced changes of thalamic input.

In contrast to the strong effect of 10-Hz TMS, 1-Hz TMS showed decreased responsiveness, along with no remodeling effects. This would support the view that low-frequency TMS facilitates suppressive mechanisms (13, 16, 20–22) and conceivably stabilizes orientation maps.

Finally, our results imply a surprising homogeneity of changes in orientation map layout after 10-Hz TMS. Note, however, that our method depicts an average population picture of upper cortical layer activity. Therefore, possibly existing subpopulations of neurons resistant to plasticity (32, 41) remain masked. Similarly, the method is blind to the possibility of involvement of distinct inhibitory cell circuits, which have been shown to change cortical state and enhance visual plasticity through disinhibition (42).

In summary, our data show that high-frequency 10-Hz TMS induces a state where visual responses are destabilized and undergo increased variability (i.e., decreased reproducibility) in orientation preference accompanied by increased excitability, most likely based on changes in excitation/inhibition balance—a potential main driving force for plastic cortical processes (43–45). In turn, the cortex may transiently be sensitized to a bias in input (23, 41, 46)—here imposed by prolonged stimulation with a single orientation—and primed to relearn connectivity patterns. Our results therefore suggest that perceptual training would be most effective immediately following high-frequency TMS application. During the immediate post-TMS phase, internal variability is produced in cortical responses (47), which may increase sensitivity to new input regularities. Plastic neuronal processes are then primed to store the newly acquired response properties. Interestingly, such a principle, that is, flexibly processing the tradeoff between internally generated variability and acquisition of novel global regularities to restructure neuronal networks, has recently been shown also for human motor-learning (48). We show here at the level of early sensory cortex that such remapping can be targeted and enhanced by specific input combined with noninvasive brain stimulation.

Materials and Methods

Experimental Design. We applied voltage-sensitive dye (VSD) imaging over primary visual cortex (V1) in adult anesthetized cats (mean age 19 mo ± 5, SD; mean body weight 3.3 kg ± 1, SD). First, we imaged the layout of orientation maps using drifting oriented gratings to determine their individual layout across cortex ("pre" conditions). After establishment of the orientation maps, repetitive transcranial magnetic stimulation (TMS) was performed over V1 for ~30 min (see below for details). In seven experiments we used 10 Hz, in five experiments we used 1 Hz, and in four experiments we used sham TMS as controls. In five out of the seven 10-Hz TMS experiments and in all other experiments with different conditions, orientation maps were measured immediately after TMS. In two 1-Hz experiments, only two (cardinal) orientations were used to measure post-TMS responsiveness. Following TMS, we stimulated with counterphase flickering gratings of an individual orientation [pseudorandomly varied across different experiments (10-Hz TMS: 2 × 90°, 1 × 0°, 2 × +45°, 2 × −45°; 1-Hz TMS: 90°, +45°, −45°; sham TMS: 90°, 0°, +45°, −45°) over ~30 min] to mimic passive, nonattentional, visual training (14, 49). Thereafter, orientation maps were continuously measured to track ongoing changes in orientation map layout (over ~2.5 h after visual stimulation, median time across experiments, over ~6 h at the longest in one experiment) until the end of the individual experiments, determined by significant decrease in fluorescence.

Surgery and Animal Preparation. Surgery and animal preparation followed our standard procedures (16, 50, 51), approved in accordance with the European Union Community Council guidelines, local government authorities [German Animal Care and Use Committee in accordance with the Deutsches Tierschutzgesetz (section 8, Abs. 1)], and the NIH guidelines. In brief, cats were initially anesthetized with ketamine (i.m., 20 mg·kg⁻¹) and xylazine (i.m., 1 mg·kg⁻¹), artificially respirated (Ugo Basile), continuously anesthetized with 0.8–1.5% isoflurane in a 1:2 mixture of O_2/N_2O, and nourished intravenously. Following surgery, paralysis was induced and maintained by Pancuronium [i.v., 0.05 mg·(kg·h)⁻¹; Inresa]. To control for eye drift, the position of the area centralis was measured repeatedly. We administered 0.4 mg·kg⁻¹ Dexamethasone i.m. and 0.05 mg·kg⁻¹ atropine sulfate, i.m., daily

Fig. 5. Unaltered maps after 1-Hz TMS. (A) The 1-Hz TMS, same stimulation protocol as for 10-Hz TMS interventions; timeline on *Top*. No changes in map layout after visual stimulation were observed [average across 11 (pre) and 13 trials (post) of a single experiment]. (B) Polar plot of preferred orientations across orientation maps [values are relative to the trained orientation (cf. Fig. 1C)]. Thin lines illustrate individual experiments (n = 3), green after 1-Hz TMS and visual stimulation (median > 140 min) and gray for preconditions; thick lines show averages. (C) Percentage of change in representation after 1-Hz TMS (mean across three experiments). (D) Across all orientations no attractive shifts were present after 1-Hz TMS and visual stimulation (cf. Fig. 2). (E) Difference between visually evoked amplitudes (average across different stimulus orientations) before and directly after 1-Hz or 10-Hz TMS interventions (n = 5 different experiments for each TMS frequency). Bars represent temporally averaged activity from 150 to 300 ms after stimulus onset. (F) Mean correlation coefficients between pairs of orientation maps (averages of resampled single-trial maps with the mean map for each orientation across experiments [bootstrap, 1,000 iterations (cf. Fig. 3E)]) after 1-Hz TMS (n = 3) and after 10-Hz TMS (n = 5). (G) Same as F for post-TMS reproducibility values. *P < 0.05, Wilcoxon rank-sum test. Error bars indicate SEM.

and 20 mg·kg^{-1} Cephazolin, i.v., twice a day. Zero-power contact lenses with a 3-mm-diameter pupil were used as protectives, and lenses were used to focus the eyes on the screen. Heart rate, intratracheal pressure, end-tidal CO_2, and body temperature were monitored. The skull was opened above area V1, the dura was removed, and a chamber was mounted. The cortex was stained for 2–3 h with voltage-sensitive dye (RH-1691), then unbound dye was washed out with artificial CSF.

VSD Optical Imaging and Preprocessing. Optical recordings were performed using the Imager 3001 (Optical Imaging Inc.) and a tandem lens macroscope (52), with 85 mm/1.2 away and 50 mm/1.2 toward subject, attached to a CCD camera (DalStar; Dalsa). For detection of changes in fluorescence the cortex was illuminated with light of wavelength 630 ± 10 nm, and emitted light

above 665 nm was collected. Recording frame rate was set to 100 Hz. The raw imaging data were preprocessed by dividing each pixel value by an average of 200-ms prestimulus activity and subsequently subtracted by the average of two blanks (i.e., recordings with an isoluminant gray screen) to remove heartbeat and respiration "artifacts." As our recordings were synchronized with the heartbeat and respiration cycles of the animal, blank subtraction effectively removes those artifacts (16, 50, 51). Altogether, these processing steps led to a unitless relative signal of fluorescence changes, denoted by ΔF/F.

Visual Stimulation. To measure visually evoked cortical responses, moving high-contrast sine-wave gratings were used (0.2 cycles/deg, 6 cycles/s, mean luminance 35 cd/m^2) with eight orientations (22.5° steps, 13 experiments), four orientations (45° steps, one experiment), or two orientations (vertical/horizontal, two experiments), including opposite-motion directions and covering a visual field of ~30° × 40°. A single trial comprised measurements of all orientations and the two blanks (presented in pseudorandom order); each stimulus recording lasted 1 s, including 200 ms prestimulus time.

For visual stimulation after TMS, flickering (10-Hz) square-wave gratings were presented with one constant orientation for 25–30 min, applied in trains of 2 s (triggered every 7 s). Michelson contrast was 0.75, and spatial frequency was 0.2 cycles/deg. Orientations were varied in different experiments (see above).

Transcranial Magnetic Stimulation. Magnetic pulses were generated by a MagStim rapid^2 stimulator (The Magstim Company Ltd.) and applied to the occipital cortex via a 90-mm circular coil (to optimize camera access) or a 70-mm figure-of-eight coil (in two experiments). Coils were covered with wet cotton compresses, ventilated by a microventilator to avoid overheating. The circular coil was placed horizontally 5–10 mm above the skull, enclosing the cranial recording chamber. To position the strongest induced electric field as close as possible to the imaged area and, at the same time, to avoid any contact with stereotactic equipment in front of the animal, the coil was placed slightly off-center with respect to the recording chamber. When a figure-of-eight coil was used, it was positioned obliquely and closest to the chamber at the imaged side. In all cases, coil position was adjusted to create an unobstructed view through the camera lens. Stimulator output was measured by a semiconductor probe based on n-type doped Ga-As heterostructure (A. Wieck, Faculty of Physics, Ruhr University Bochum, Germany). The stimulator generated 400 μs biphasic magnetic pulses; output was set to 60% of maximal intensity, corresponding to peak magnetic field strength of 0.2–0.5 Tesla. Measurements in spherical models of different sizes demonstrated decreasing electric field strength with decreasing brain sizes (53). Using a circular coil with similar properties to the one used here, Weissman et al. (43) estimated that the electric field strength in a brain of the size of a cat was ~30–50 V m^{-1} lower compared with the human brain size. Thus, under the given constraints of a sphere, we induced an electric field of 25–80 V m^{-1}.

Repetitive TMS was applied for a period of 25–30 min. The 10-Hz protocol contained high-frequency sequences of five pulses triggered every 7 s, with 3- to 5-min breaks to avoid overheating of the coil or to exchange with a spare. Sham TMS was performed, during which the coil was positioned at a 45° angle from horizontal, >10 cm away from the head of the animal, under otherwise identical experimental conditions to the 10-Hz protocol. For the low-frequency (1-Hz) protocol, pulses were applied in three trains, each lasting 7 min, summing up to 1,250 pulses.

Data Analysis and Statistics. To calculate orientation maps, images were first averaged over time frames (150–600 ms after stimulus onset). To eliminate high-frequency noise and low-frequency components, images were band-pass-filtered (0.225–1.75 cycles × mm^{-1}). On average, results were summarized across 11.6 ± 4.66 SD trials. We tried to keep the number of trials as low as possible to minimize time between TMS and visual stimulation and to retain dye-bleaching at a minimum over the entire time course of the experiments. Trials where responses were below significance (i.e., below 2 SD of prestimulus time or below 2 SD of blank conditions) were excluded from analysis. If two or more consecutive trials were below significance during the final phase of the measurements (i.e., after TMS protocols and visual stimulation), most likely indicating decreased signal-to-noise due to dye-bleaching (54), experiments were terminated. Edges of images were cropped to exclude noisy border regions. One sham TMS experiment was excluded from map analysis because of an initial strong bias in orientation representation toward cardinal orientations.

Orientation maps were obtained by computing the vector sum of the responses at each pixel in the image to all orientations and displaying the angle of the resulting vector in color (55, 56). Reproducibility maps were calculated across single-trial responses (57). Our main assumption here is that a selective response should be reliable, i.e., it should code for similar orientation in most of the trials (*SI Appendix, SI Methods*).

1. Merzenich MM, et al. (1983) Progression of change following median nerve section in the cortical representation of the hand in areas 3b and 1 in adult owl and squirrel monkeys. *Neuroscience* 10:639–665.
2. Poggio T, Fahle M, Edelman S (1992) Fast perceptual learning in visual hyperacuity. *Science* 256:1018–1021.
3. Das A, Gilbert CD (1995) Long-range horizontal connections and their role in cortical reorganization revealed by optical recording of cat primary visual cortex. *Nature* 375:780–784.
4. Barker AT, Jalinous R, Freeston IL (1985) Non-invasive magnetic stimulation of human motor cortex. *Lancet* 1:1106–1107.
5. Pascual-Leone A, Walsh V, Rothwell J (2000) Transcranial magnetic stimulation in cognitive neuroscience–Virtual lesion, chronometry, and functional connectivity. *Curr Opin Neurobiol* 10:232–237.
6. Hallett M (2000) Transcranial magnetic stimulation and the human brain. *Nature* 406:147–150.
7. Walsh V, Cowey A (2000) Transcranial magnetic stimulation and cognitive neuroscience. *Nat Rev Neurosci* 1:73–79.
8. Thompson B, Mansouri B, Koski L, Hess RF (2008) Brain plasticity in the adult: Modulation of function in amblyopia with rTMS. *Curr Biol* 18:1067–1071.
9. Waterston ML, Pack CC (2010) Improved discrimination of visual stimuli following repetitive transcranial magnetic stimulation. *PLoS One* 5:e10354.
10. Romei V, Gross J, Thut G (2010) On the role of prestimulus alpha rhythms over occipito-parietal areas in visual input regulation: Correlation or causation? *J Neurosci* 30:8692–8697.
11. Siebner HR, et al. (2009) Consensus paper: Combining transcranial stimulation with neuroimaging. *Brain Stimul* 2:58–80.
12. Gersner R, Kravetz E, Feil J, Pell G, Zangen A (2011) Long-term effects of repetitive transcranial magnetic stimulation on markers for neuroplasticity: Differential outcomes in anesthetized and awake animals. *J Neurosci* 31:7521–7526.
13. Freitas C, Farzan F, Pascual-Leone A (2013) Assessing brain plasticity across the lifespan with transcranial magnetic stimulation: Why, how, and what is the ultimate goal? *Front Neurosci* 7:42.
14. Seitz AR, Dinse HR (2007) A common framework for perceptual learning. *Curr Opin Neurobiol* 17:148–153.
15. Grinvald A, Hildesheim R (2004) VSDI: A new era in functional imaging of cortical dynamics. *Nat Rev Neurosci* 5:874–885.
16. Kozyrev V, Eysel UT, Jancke D (2014) Voltage-sensitive dye imaging of transcranial magnetic stimulation-induced intracortical dynamics. *Proc Natl Acad Sci USA* 111:13553–13558.
17. Bonhoeffer T, Grinvald A (1991) Iso-orientation domains in cat visual cortex are arranged in pinwheel-like patterns. *Nature* 353:429–431.
18. Dragoi V, Sharma J, Sur M (2000) Adaptation-induced plasticity of orientation tuning in adult visual cortex. *Neuron* 28:287–298.
19. Sharon D, Grinvald A (2002) Dynamics and constancy in cortical spatiotemporal patterns of visual processing. *Science* 295:512–515.
20. Kim T, Allen EA, Pasley BN, Freeman RD (2015) Transcranial magnetic stimulation changes response selectivity of neurons in the visual cortex. *Brain Stimul* 8:613–623.
21. Robertson EM, Théoret H, Pascual-Leone A (2003) Studies in cognition: The problems solved and created by transcranial magnetic stimulation. *J Cogn Neurosci* 15:948–960.
22. Lenz M, et al. (2016) Repetitive magnetic stimulation induces plasticity of inhibitory synapses. *Nat Commun* 7:10020.
23. Schuett S, Bonhoeffer T, Hübener M (2001) Pairing-induced changes of orientation maps in cat visual cortex. *Neuron* 32:325–337.
24. Godde B, Leonhardt R, Cords SM, Dinse HR (2002) Plasticity of orientation preference maps in the visual cortex of adult cats. *Proc Natl Acad Sci USA* 99:6352–6357.
25. Kaas JH, et al. (1990) Reorganization of retinotopic cortical maps in adult mammals after lesions of the retina. *Science* 248:229–231.
26. Gilbert CD, Wiesel TN (1992) Receptive field dynamics in adult primary visual cortex. *Nature* 356:150–152.
27. Young JM, et al. (2007) Cortical reorganization consistent with spike timing-but not correlation-dependent plasticity. *Nat Neurosci* 10:887–895.
28. Giannikopoulos DV, Eysel UT (2006) Dynamics and specificity of cortical map reorganization after retinal lesions. *Proc Natl Acad Sci USA* 103:10805–10810.
29. Holtmaat A, Svoboda K (2009) Experience-dependent structural synaptic plasticity in the mammalian brain. *Nat Rev Neurosci* 10:647–658.
30. Keck T, et al. (2008) Massive restructuring of neuronal circuits during functional reorganization of adult visual cortex. *Nat Neurosci* 11:1162–1167.
31. Cirillo G, et al. (2017) Neurobiological after-effects of non-invasive brain stimulation. *Brain Stimul* 10:1–18.
32. Rose T, Jaepel J, Hübener M, Bonhoeffer T (2016) Cell-specific restoration of stimulus preference after monocular deprivation in the visual cortex. *Science* 352:1319–1322.
33. Niell CM, Stryker MP (2010) Modulation of visual responses by behavioral state in mouse visual cortex. *Neuron* 65:472–479.
34. Calford MB, Schmid LM, Rosa MG (1999) Monocular focal retinal lesions induce short-term topographic plasticity in adult cat visual cortex. *Proc Biol Sci* 266:499–507.
35. Barron HC, Vogels TP, Behrens TE, Ramaswami M (2017) Inhibitory engrams in perception and memory. *Proc Natl Acad Sci USA* 114:6666–6674.
36. Jaepel J, Hübener M, Bonhoeffer T, Rose T (2017) Lateral geniculate neurons projecting to primary visual cortex show ocular dominance plasticity in adult mice. *Nat Neurosci* 20:1708–1714.
37. Cash RF, Ziemann U, Murray K, Thickbroom GW (2010) Late cortical disinhibition in human motor cortex: A triple-pulse transcranial magnetic stimulation study. *J Neurophysiol* 103:511–518.
38. Cash RF, Murakami T, Chen R, Thickbroom GW, Ziemann U (2016) Augmenting plasticity induction in human motor cortex by disinhibition stimulation. *Cereb Cortex* 26:58–69.
39. Patterson CA, Wissig SC, Kohn A (2013) Distinct effects of brief and prolonged adaptation on orientation tuning in primary visual cortex. *J Neurosci* 33:532–543.
40. Li B, et al. (2017) Lifting the veil on the dynamics of neuronal activities evoked by transcranial magnetic stimulation. *eLife* 6:e30552.
41. Clopath C, Bonhoeffer T, Hübener M, Rose T (2017) Variance and invariance of neuronal long-term representations. *Philos Trans R Soc Lond B Biol Sci* 372:20160161.
42. Fu Y, Kaneko M, Tang Y, Alvarez-Buylla A, Stryker MP (2015) A cortical disinhibitory circuit for enhancing adult plasticity. *eLife* 4:e05558.
43. Isaacson JS, Scanziani M (2011) How inhibition shapes cortical activity. *Neuron* 72:231–243.
44. Letzkus JJ, Wolff SB, Lüthi A (2015) Disinhibition, a circuit mechanism for associative learning and memory. *Neuron* 88:264–276.
45. Bavelier D, Levi DM, Li RW, Dan Y, Hensch TK (2010) Removing brakes on adult brain plasticity: From molecular to behavioral interventions. *J Neurosci* 30:14964–14971.
46. Froemke RC, Merzenich MM, Schreiner CE (2007) A synaptic memory trace for cortical receptive field plasticity. *Nature* 450:425–429.
47. Pasley BN, Allen EA, Freeman RD (2009) State-dependent variability of neuronal responses to transcranial magnetic stimulation of the visual cortex. *Neuron* 62:291–303.
48. Wu HG, Miyamoto YR, Gonzalez Castro LN, Ölveczky BP, Smith MA (2014) Temporal structure of motor variability is dynamically regulated and predicts motor learning ability. *Nat Neurosci* 17:312–321.
49. Seitz A, Watanabe T (2005) A unified model for perceptual learning. *Trends Cogn Sci* 9:329–334.
50. Nortmann N, Rekauzke S, Onat S, König P, Jancke D (2015) Primary visual cortex represents the difference between past and present. *Cereb Cortex* 25:1427–1440.
51. Rekauzke S, et al. (2016) Temporal asymmetry in dark-bright processing initiates propagating activity across primary visual cortex. *J Neurosci* 36:1902–1913.
52. Ratzlaff EH, Grinvald A (1991) A tandem-lens epifluorescence macroscope: Hundred-fold brightness advantage for wide-field imaging. *J Neurosci Methods* 36:127–137.
53. Weissman JD, Epstein CM, Davey KR (1992) Magnetic brain stimulation and brain size: Relevance to animal studies. *Electroencephalogr Clin Neurophysiol* 85:215–219.
54. Shoham D, et al. (1999) Imaging cortical dynamics at high spatial and temporal resolution with novel blue voltage-sensitive dyes. *Neuron* 24:791–802.
55. Blasdel GG, Salama G (1986) Voltage-sensitive dyes reveal a modular organization in monkey striate cortex. *Nature* 321:579–585.
56. Swindale NV (1998) Orientation tuning curves: Empirical description and estimation of parameters. *Biol Cybern* 78:45–56.
57. Grabska-Barwińska A, Ng BS, Jancke D (2012) Orientation selective or not?–Measuring significance of tuning to a circular parameter. *J Neurosci Methods* 203:1–9.

NEUROSCIENCE